Microstructure evolution of Ti_3SiC_2 compound cathodes during reactive cathodic arc evaporation

J. Q. Zhu[a)]
Nanostructured Materials, Department of Physics, Chemistry, and Biology (IFM), Linköping University, SE-581 83 Linköping, Sweden

A. O. Eriksson
Thin Film Physics Division, Department of Physics, Chemistry, and Biology (IFM), Linköping University, SE-581 83 Linköping, Sweden

N. Ghafoor
Nanostructured Materials, Department of Physics, Chemistry, and Biology (IFM), Linköping University, SE-581 83 Linköping, Sweden

M. P. Johansson
Nanostructured Materials, Department of Physics, Chemistry, and Biology (IFM), Linköping University, SE-581 83 Linköping, Sweden and SECO Tools AB, SE-737 82 Fagersta, Sweden

G. Greczynski, L. Hultman, and J. Rosén
Thin Film Physics Division, Department of Physics, Chemistry, and Biology (IFM), Linköping University, SE-581 83 Linköping, Sweden

M. Odén
Nanostructured Materials, Department of Physics, Chemistry, and Biology (IFM), Linköping University, SE-581 83 Linköping, Sweden

(Received 26 December 2010; accepted 28 February 2011; published 23 March 2011)

The microstructure evolution and compositional variation of Ti_3SiC_2 cathode surfaces during reactive cathodic arc evaporation are presented for different process conditions. The results show that phase decomposition takes place in the near-surface region, resulting in a 5–50 μm thick converted layer that is affected by the presence of nitrogen in the deposition chamber. This layer consists of two different sublayers, i.e., 1–20 μm thick top layer with a melted and resolidified microstructure, followed by a 4–30 μm thick transition layer with a decomposed microstructure. The converted layer contains a polycrystalline TiC_x phase and trace quantities of Si-rich domains with $Ti_5Si_3(C)$ at their interface. The arc discharge causes Si redistribution in the two regions of the layer, whose Si/(Ti+Si) ratio is higher in the top region and lower in the transition region compared to the virgin material. © *2011 American Vacuum Society.* [DOI: 10.1116/1.3569052]

I. INTRODUCTION

Hard coatings based on the Ti–Si–C–N system are promising candidates for wear-resistant layers on cutting tools.[1,2] Coatings from this material system have been synthesized by chemical vapor deposition[1,2] and magnetron sputtering techniques[3] in the past decade, while only a limited number of reports exist on the behavior of Ti–Si–C–N coatings grown by reactive cathodic arc evaporation (CAE).[4,5] In order to achieve a high performance coating that exhibits high thermal stability and hardness, the Si and C contents have to be tuned with high accuracy.[4] Hence, the demands on the control of the deposition process are increasing, which includes the processes on the cathode surface for CAE.

When growing Ti–Si–C–N coating by CAE, one can choose different cathode configurations in terms of cathode materials, i.e., elemental, binary (Ti–Si), or ternary (Ti–Si–C) compounds. We have recently shown that the choice of cathode material influences the physical evaporation process and eventually the microstructure and composition of the coatings.[6] Binary Ti–Si cathodes are mostly fabricated as an alloy and its microstructure will strongly depend on the Si content. Ternary Ti–Si–C cathodes are produced as multiphase alloys, composites, and for specific compositions as a single-phase compound with trace impurity phase, e.g., the MAX phase Ti_3SiC_2 with TiC.[7] The Ti_3SiC_2 compound is of special interest since it possesses unique properties,[7,8] including higher electrical and thermal conductivities, similar thermal shock resistance, and better machinability compared to the Ti–Si alloys. Therefore, it could be an attractive cathode material for reactive cathodic arc evaporation synthesis of Ti–Si–C–N coatings.

In the Ti–Si–C ternary system at thermodynamic equilibrium,[9] Ti_3SiC_2 coexists with several binary phases, including TiC, Ti_5Si_3, SiC, and $TiSi_2$. The thermal stability and phase decomposition of Ti_3SiC_2 depend on impurities and the environment. It has been reported that Ti_3SiC_2 decomposes at 900 °C in the presence of Cu,[10] at 1300 °C in a C-crucible,[11] and above 1800 °C for a sufficiently pure sample in air.[12] It is unknown how the Ti_3SiC_2 cathode surface evolves, specifically if transformation or decomposition

a)Author to whom correspondence should be addressed; electronic mail: zhu@ifm.liu.se

of the Ti_3SiC_2 phase occurs under the condition of high current discharging during the reactive arc process. However, it is known that the arc process is influenced by the microstructure and composition of the cathode surface,[13–18] and thus a detailed investigation of the cathode microstructure evolution under these conditions is needed.

In this work, the microstructural evolution of the MAX Ti_3SiC_2 cathodes evaporated at different conditions in terms of pressure and arc current is reported. The results show that phase decomposition occurs on the cathode surface, forming a converted layer with depth varying microstructure and compositions depending on the nitrogen pressure. The formation mechanism is also discussed.

II. EXPERIMENTAL DETAILS

Maxthal® Ti_3SiC_2, fabricated by Kanthal AB, Sweden, was used as the cathode material for reactive cathodic arc deposition of Ti–Si–C–N coatings in a commercial Sulzer compact arc system.[19] The density of Maxthal® Ti_3SiC_2 is $\sim 4.34\ g/cm^3$, which is $\sim 96\%$ of the theoretical density of Ti_3SiC_2. The cathodes were fabricated from a larger slab and shaped into 26 mm thick disks with a diameter of 63 mm. All experiments were conducted for 1 h to reach steady-state process conditions at different arc currents (50, 70, and 90 A) and N_2 partial pressures (0, 0.5, 1.2, and 2.0 Pa, respectively). During arc evaporation, the cathodes were water cooled through a Cu-backing plate. The arc voltage was initially 16 V during the start-up stage and then it stabilized between 17 and 19 V, whereas the arc current fluctuated within ± 2.5 A around the running currents of 50, 70, and 90 A. Specimens with dimensions of $10 \times 10 \times 5\ mm^3$ were then cut out from the worn cathode surfaces and used to characterize the morphology, microstructure, and chemical bonding structure of the surface region with respect to the process conditions used.

The surface roughness was measured by a TalySurf PGI840 profilometer. The structures of the evaporated surfaces were investigated by grazing incidence x-ray diffraction utilizing a Philips diffractometer and Cu $K\alpha$ radiation at an incidence angle of 2°. The worn surface plan view and cross sections were recorded with scanning electron microscopy (SEM) using a LEO 1550 FEG-SEM microscope operated at 5 kV.

The microstructural and compositional investigations were carried out in transmission electron microscopy (TEM) and scanning transmission electron microscopy (STEM) modes using a Tecnai G^2 20 U-Twin 200 FEG TEM instrument operated at 200 kV. STEM micrographs were obtained with a high-angle annular dark field detector with a 1.9 Å probe. The electron energy loss spectroscopy (EELS) and energy dispersive spectroscopy (EDX) maps were recorded with a pixel size of $5 \times 5\ nm^2$ with a dwell time of 1 s. Cross-sectional samples for TEM or STEM were prepared by focused ion beam (FIB) technique using a Carl Zeiss CrossBeam 1540 EsB system. The detailed description of the TEM sample preparation procedure by FIB can be found elsewhere.[20]

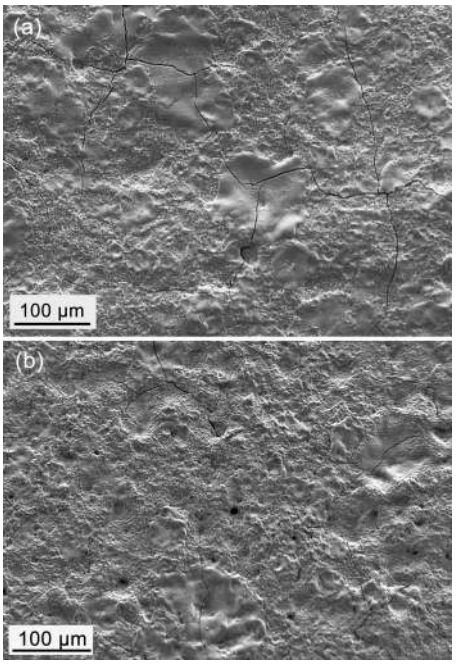

FIG. 1. Scanning electron micrograph of worn MAX Ti_3SiC_2 cathode surface evaporated in (a) the reactive mode of 50 A arc current and 2 Pa N_2 pressure and (b) nonreactive mode of 50 A arc current and 0 Pa N_2 pressure.

X-ray photon spectroscopy (XPS) was performed in a Scienta ESCA200 spectrometer from VG Scienta using a monochromatized Al $K\alpha$ x-ray radiation with a photon energy of $h\nu = 1486.6$ eV. The experimental conditions were such that the full width at half maximum of the gold, Au($4f7/2$), line was 0.65 eV. All surfaces were ultrasonically cleaned with acetone/isopropanol for 10 min prior to XPS measurements. The XPS spectra were taken on as-received samples, i.e., without any sputter etch, in order not to risk sputter-induced chemical modifications. The graphite C 1*s* position at 284.6 eV was used as reference for the energy calibration and a Shirley-type background subtraction was used in the data analysis.

III. RESULTS

A. Overview of the worn cathode surfaces

Figure 1 shows scanning electron micrographs of the worn cathode surfaces evaporated in (a) a reactive mode with 50 A arc current and 2 Pa N_2 pressure and (b) a nonreactive mode with 50 A arc current and 0 Pa N_2 pressure. The worn cathode surfaces are covered with craters, which are a remnant trail of the arc spots. These craters, ranging from ~ 2 to 50 μm in diameter, are overlapping and form groups with diameters exceeding 100 μm. Cracks are apparent on both worn surfaces. A similar appearance of the cathode surface regarding the surface morphology and crater size distribution is observed for other process conditions, i.e., with N_2 pressures of 0, 0.5, 1.2, and 2 Pa at an arc current of 50 A, and with arc currents of 50, 70, and 90 A at N_2 pressure of 2 Pa,

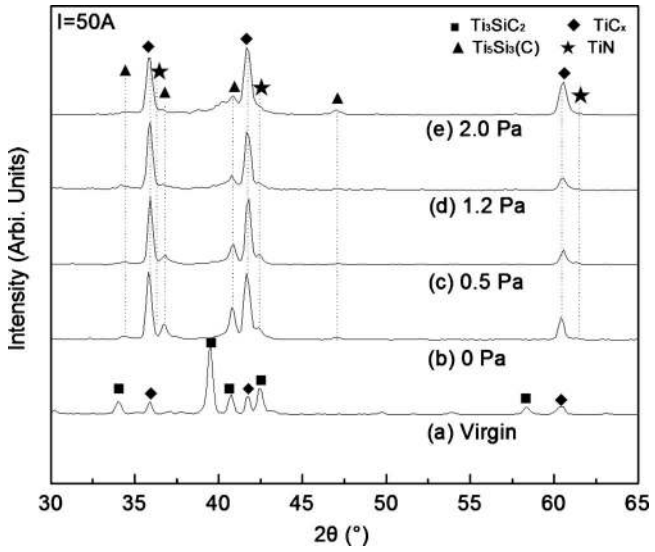

FIG. 2. X-ray diffractograms from (a) the virgin MAX Ti_3SiC_2 cathode surface and [(b)–(e)] the worn MAX Ti_3SiC_2 cathode surface: evaporated in a N_2 pressure of (b) 0 Pa, (c) 0.5 Pa, (d) 1.2 Pa, and (e) 2.0 Pa at 50 A current, respectively.

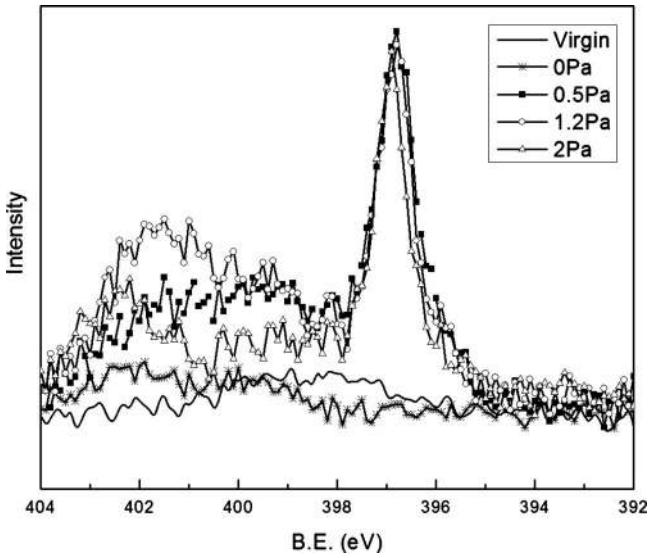

FIG. 3. N 1*s* region of the XPS spectrum from the fresh cathode surface and the ones worn at different nitrogen pressure: 0, 0.5, 1.2, and 2.0 Pa, respectively.

respectively. The surface roughness R_a of worn cathodes is 2.8 μm run in reactive conditions and 7.1 μm for the cathodes run in nonreactive conditions.

Figure 2 shows grazing incidence x-ray diffractograms from (a) the virgin and [(b)–(e)] the worn surfaces of Ti_3SiC_2 cathode, processed at a fixed arc current of 50 A and different N_2 pressures. The diffraction peaks in Fig. 1(a) are identified to be from Ti_3SiC_2 and TiC_x, i.e., the polycrystalline virgin cathode material contains Ti_3SiC_2 with 14.7 wt % TiC_x, for which x could range from 0.47 to 0.97.[21] After arcing, the worn cathode surfaces mainly consist of TiC_x and a small amount of $Ti_5Si_3(C)$. The $Ti_5Si_3(C)$ phase, which is a solid solution of Ti_5Si_3 and C, appears in a comparably small amount, independent of the arc evaporation conditions. In the case of reactive conditions, the diffractograms show additional minor peaks of TiN. Increasing the N_2 pressure from 0.5 to 2.0 Pa results in a more intense TiC_x signal, while the $Ti_5Si_3(C)$ decreases, i.e., the higher the N_2 pressure, the more TiC_x forms on the cathode surface. The diffractograms from cathodes operated at arc currents of 50, 70, and 90 A (not shown) were similar to that shown in Fig. 2(c).

The XPS N 1*s* spectra of the worn Ti_3SiC_2 cathode surfaces, which are normalized to the corresponding Ti 2*p* spectral peaks, are shown in Fig. 3. A distinct peak that appears at 396.8 eV for all surfaces that were worn in the N_2 atmosphere corresponds to the Ti–N bond in TiN. A variation in the nitrogen pressure from 0.5 to 2.0 Pa does not result in any significant changes to the binding energy or the intensity of this spectral feature. The broad contributions present at the higher binding energy (between 401 and 402 eV) can be assigned to various carbon-nitride bonds that are likely to appear as a final product on reactively sputtered Ti_3SiC_2 cathode surface.

B. Microstructure evolution of the cathode surface when operated in a reactive mode

Cross-sectional (X) SEM and TEM imaging of the worn cathode surfaces at different reactive arc conditions were found to exhibit similar morphologies. A converted layer covers the cathode surface on top of the virgin material. Figure 4 shows representative XSEM micrographs of the cathode evaporated at 2 Pa nitrogen pressure and 50 A arc current.

The overview of a polished cross section in Fig. 4(a) reveals a variation in depth of the grain size. In the first 3–4 μm below the surface, region I, 100–500 nm equiaxed grains dominate the microstructure. Region II contains grainlike features that appear to be layered. Region II consists of 3–10 μm grains, with a shape similar to what was observed

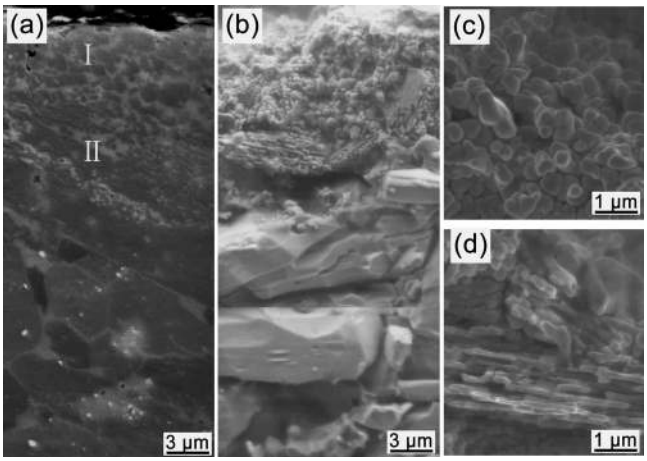

FIG. 4. Cross-sectional scanning electron micrographs of the worn cathode surface evaporated in 2 Pa N_2 pressure at 50 A arc current: (a) overview of the polished sample, (b) overview of the fine etched sample, high magnification images of the (c) top surface region and (d) transition region from (b).

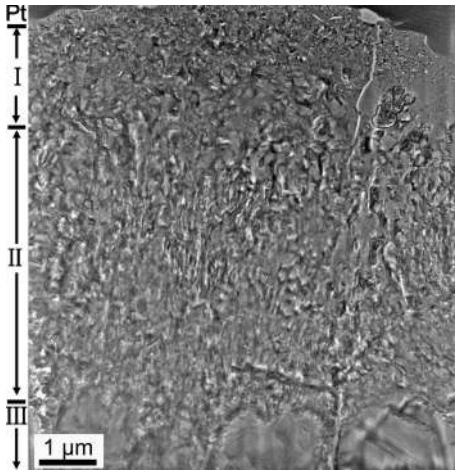

FIG. 5. Cross-sectional scanning transmission electron micrographs of the worn cathode surface evaporated in 2 Pa N_2 pressure at 50 A arc current.

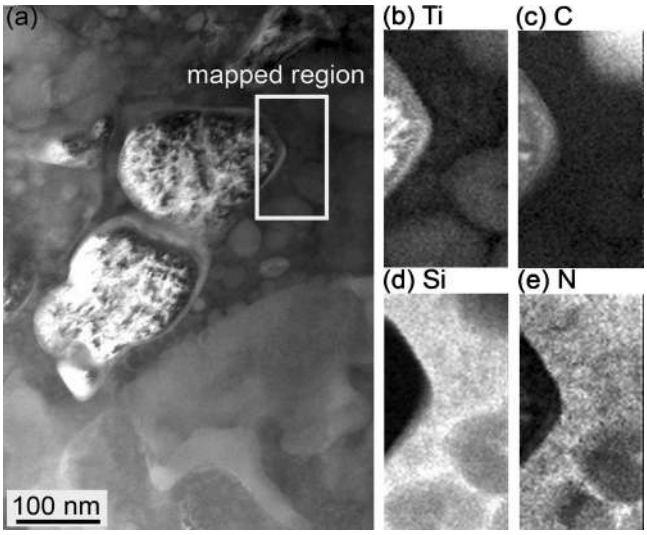

FIG. 6. Scanning transmission electron micrograph with EELS and EDX maps of the marked area in region I (Fig. 3) from the 2 Pa-50 A evaporated MAX cathode surface: (a) STEM image of the selected mapped area, (b) Ti EDX map, (c) C EELS map, (d) Si EDX map, and (e) N EELS map.

for the Ti_3SiC_2 grains of the virgin material. Figure 4(b) gives an overview of how the converted layer appear after chemical etching, and Figs. 4(c) and 4(d) are magnifications of regions I and II, respectively. Here, it can be seen that the grains in region I are actually aggregates of smooth and nearly spherically shaped grains, approximately 500 nm in diameter, and that the grainlike features in region II are 5–10 μm wide and 300–500 nm thick. EDX elemental quantification of the Si/(Si+Ti) ratio based on an average of data collected from 15 different locations inside each region resulted in values of $27 \pm 2\%$ and $23 \pm 3\%$ for regions I and II, respectively, while the virgin cathode shows a value of $26 \pm 1\%$.

Figure 5 shows a XTEM micrograph of the converted layer. In the near-surface region (region I), the converted layer contains nanosized grains, which gradually increase in size from 20 to 150 nm. Thereafter, a 3 μm thick transition zone (region II) consists of vertically aligned and elongated grains.

Figure 6 shows a STEM image obtained from region I and taken at short camera length providing dominantly z-contrast image information, i.e., the bright area indicates the presence of heavier elements and vice versa.

Figure 6(a) shows a random distribution of the grains and their sizes vary from 10 to 150 nm. The larger bright grains presumably contain Ti and are typically covered by an outer grayish shell. A 200×500 nm^2 area, which includes a part of a lager grain and several small ones was selected for compositional analysis. The EDX and EELS maps in Figs. 6(b)–6(d) reveal that the large grains contain both Ti and C, which is consistent with TiC_x. The gray outer shell contains Ti, Si, and C with Ti:Si ratio of $\sim 5:3$, consistent with the $Ti_5Si_3(C)$ phase. N is present throughout the structure at various contents except for the larger TiC_x grain, which are N-free [see Fig. 6(e)]. Small amounts of TiN could thus exist in this region in addition to a solid solution of the type $Ti_5Si_3(C,N)$. Combined with the phase information from GI-XRD results in Fig. 2, and the elemental maps we conclude that region I consists of TiC_x, $Ti_5Si_3(C)$, and TiN grains.

Figure 7 shows a STEM image with corresponding elemental maps from region II. The STEM image in Fig. 7(a) indicates that the layered grainlike features seen in Fig. 4 contains ellipsoidally shaped grains within a matrix phase. No N signal is detected from this region, while a strong Ti

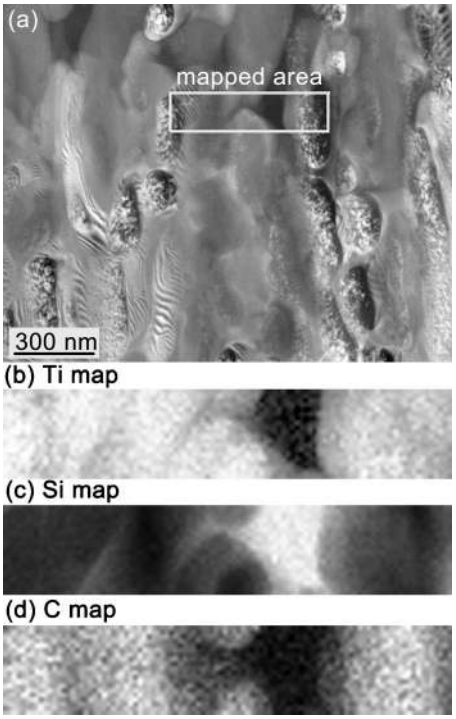

FIG. 7. Scanning transmission electron micrograph with EDX and EELS maps of the marked area in region II (Fig. 3) from the 2Pa-50A evaporated MAX cathode surface: (a) STEM image of the selected area, (b) Ti EDX map, (c) Si EDX map, and (d) C EELS map.

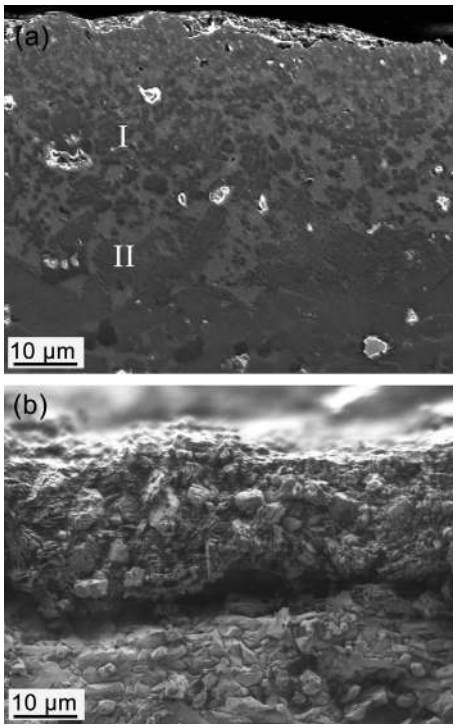

FIG. 8. Cross-sectional overview scanning electron micrograph of the nonreactive worn cathode surface: (a) the polished sample and (b) the etched sample.

signal is detected everywhere, as shown in Fig. 7(b). The Si map [Fig. 7(c)] shows that some grains are Si-rich and others containing C are Si depleted. EDX quantification analysis in the Si enriched domains, which is the very light region in Fig. 7(c), show that the atomic ratio of Si/Ti varies between 2.5 and 1, indicating a mixture of Si and titanium silicide phases. At the boundaries between Ti- and Si-rich grains, a gradient in the distribution of the Ti, Si, and C elements is seen. In this gradient region, a Ti/Si ratio of ~5:3 is recorded. Hence, the ellipsoidal grains in region II consists of TiC_x- and Si-rich domains, with a grain boundary phase with a composition close in to $Ti_5Si_3(C)$.

XSEM samples prepared from cathode surfaces exposed to different nitrogen pressures and arc currents show similar microstructure, suggesting that 0.5 Pa nitrogen pressure is sufficient to saturate the cathode surface in terms of nitrogen.

C. Microstructure evolution of the cathode surface when operated in a nonreactive mode

Figure 8 is a XSEM image of nonreactively worn cathode surface. Figure 8(a) shows a depth variation in the microstructure similar to the ones seen for cathodes operated in a reactive mode, i.e., a top surface region I with equiaxed grains, and a transition region (region II) with layered grainlike features, to the virgin Ti_3SiC_2 grains. The SEM image of the etched cross section in Fig. 8(b) reveals a converted layer, which is approximately 15–50 μm thick, i.e., three to five times thicker than in the reactive case.

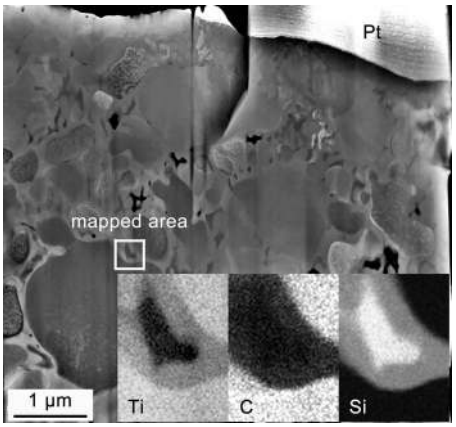

FIG. 9. Cross-sectional transmission electron micrograph of a FIB sample from nonreactive worn cathode surface at an arc current of 50 A with EDX element map of Ti, Si, and EELS element map of C. The notch near the surface is a damage effect from FIB sample preparation.

The microstructural and compositional information of the converted layer are shown in Fig. 9. The cross section contains the first 4.5 μm of the converted layer nearest the surface. The grains in the converted layer are irregular in shape and have a wider size distribution, ranging from 0.1 to 1.5 μm, compared to the converted layers in the reactive case. An area with parts from grains of different sizes was selected for elemental mapping. From the edge to the center of the mapped area, both Ti and C show a decreasing gradient distribution, while Si exhibits the inverse trend. The area rich in C contains no Si and vice versa. Hence, a similar microstructure, as seen in the reactive case, is also present here, i.e., a mixture of the TiC_x and titanium silicide grains, with $Ti_5Si_3(C)$ as a grain boundary phase.

IV. DISCUSSION

The microstructure and properties of the Ti–Si–C–N coatings deposited from these Ti_3SiC_2 compound cathodes are reported elsewhere.[6] A large variety of the coating composition and microstructures depending on the N-partial pressure were observed. Consequently, the recorded hardness varied between 20 and 50 GPa.

The results of this work show that the Ti_3SiC_2 compound cathode decomposes during arc evaporation, forming a converted surface layer that differs depending on the different process conditions. In general, the converted layer consists of two regions. A top (near-surface) region I containing 20–150 nm equiaxed TiC grains in a matrix of silicide phases, which are either $Ti_5Si_3(C)$ or $Ti_5Si_3(C)$ encapsulated with a titanium silicide phase with varying Ti/Si ratio. A transition region II follows below region I. It contains layered TiC_x grains, ranging in size from 3 to 10 μm in length and 300–500 nm in thickness, in a Ti_5Si_3C matrix and a small amount of Si-rich domains. In addition, when the cathodes were operated in a reactive mode, minor quantities of TiN exist in region I of the converted layer. It is also likely that $Ti_5Si_3(C,N)$ forms at the grain boundaries since the solubil-

ity of N in Ti_5Si_3 can be up to 11 mol %,[22] existing as Ti_6–N cluster by incorporating the N in the octahedral sites.

The formed microstructure and composition variations of the converted layer, both in nonreactive and reactive modes, are caused by the high thermal energy input from the arc through the cathode spots. The active cathode spots during arc discharging could generate temperatures above 15 000 K (Ref. 23) in the near spot region and thus cause local melting. After the spot extinguishes, the near-surface molten region rapidly solidifies due to the efficient water cooling of the cathodes. Such fast cooling process limits the solid state elemental diffusion needed for reformation of the Ti_3SiC_2 phase. The diffusion-controlled solid state reaction of Ti_3SiC_2 is known to require sufficient time at elevated temperatures.[24] Instead, the fast solidification process of the molten region is initially dominated by grain nucleation and limited grain growth of TiC_x and the concurrent formation of the $Ti_5Si_3(C)$ matrix. The presence of TiC_x and $Ti_5Si_3(C)$ phases is expected based on the Ti–Si–C phase diagram, where TiC_x with the highest melting temperature forms first with a low solubility of Si.[25,26] Both these phases have also been reported to form as intermediate phases during formation and decomposition of Ti_3SiC_2.[24,27,28]

The transition zone, region II, does probably not completely melt during the evaporation process since the observed layered regions resembles the virgin Ti_3SiC_2 grains in terms of size and shape. Instead, region II is exposed to high temperature spikes during and right after the discharge due to inward heat conductions from the surface. The individual arc events occurs within a time scale from nanoseconds to microseconds[23] and generates local heating, which are effectively quenched and rapidly dissociated. Hence, the short arc-induced time thermal spikes are apparently sufficient for phase decomposition.

The decomposition of Ti_3SiC_2 is initiated by outdiffusion of Si due to the weak Ti–Si metallic bonds in comparison to the Ti–C bonds,[7] which is expected to occur in region II. The remaining Ti_3C_2 domains transform into TiC_x (with $x=0.67-1$) through relaxation and detwinning.[7] This transformation is likely to have a crystallographic relationship with the Ti_3C_2 structure and hence responsible for the layered appearance. The outdiffusion of the Si results in formation of Si enriched domains, which are dispersed both at the original and newly formed TiC_x grain boundaries and are encapsulated by a Ti_5Si_3C shell. The crystal structure of the Si-rich domains, containing only Ti and Si signal and with Si/Ti ratio from 1 to 2.5, could not be resolved by XRD or electron diffraction due to their thin nature and low volume fraction. Based on the phase diagram, a mixture of Si, TiSi, and $TiSi_2$ is expected, all of which contain more than 50% Si. Figure 10 is a schematic illustration of the recorded elemental profiles of Ti, Si, and C across a grain boundary in region II, summarized from Figs. 7 and 9. The gradual change in concentrations of the elements supports a diffusion driven formation mechanism. The lower melting temperature of titanium silicides and their solid solutions, and the smooth shape

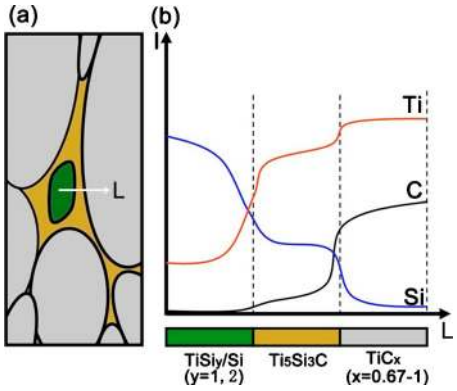

FIG. 10. (Color online) Schematic illustration of the element's concentration in the Si-rich/$Ti_5Si_3(C)$/TiC_x region.

of the ellipsoidal grains in region II suggest that these phases were in a molten state for some period even in region II.

The average Si concentrations differ in the two regions of the converted layer, i.e., higher in region I and lower in region II compared to the virgin cathode. The expected reason of the Si enrichment at the top region is that the arc discharge built up a region (I+II) with a steep temperature gradient from the cathode surface into the bulk material and causes a continuous Si diffusion toward the surface. In addition, electromigration of the cathode materials, generated by the applied electrical field, could possibly contribute to the Si redistribution as well.

The nitriding mechanisms of the Ti_3SiC_2 cathode during reactive arc evaporation can be explained by N being incorporated in the near-surface region by the redeposition of nitrided macroparticles during arcing.[17] N is thus located in the TiN or $Ti_5Si_3(C,N)$ phases of region I, which is shown by XPS, XRD, and EELS. Increasing the nitrogen pressure from 0 to 2.0 Pa results in a gradual increase of the TiC_x phase since N is incorporated into TiC to form a solid solution, $Ti(C_x,N)$. This occurs at the expense of $Ti_5Si_3(C)$ since Si loss is known to occur through evaporation when Ti_3SiC_2 is heated in a nitrogen atmosphere.[8,29,30]

The change in thickness of the converted layer between reactive and nonreactive modes is primarily an effect of the difference in the arc spot lifetime. Generally, in nonreactive evaporation single arc spot events have a longer duration compared to the reactive case. The longer time period a single arc spot stays in one location, the wider and deeper the heat influences the near-surface region of the cathode. Variation in the arc current has, however, negligible influence on the surface evolution in these experiments. This is not surprising since the lowest arc current, 50 A, employed here is already sufficient to trigger a molten state, which dictates the microstructure evolution.

V. CONCLUSIONS

The microstructure of the Maxthal® Ti_3SiC_2 cathode surfaces is found to evolve when used for deposition of Ti–Si–C–N quaternary hard coatings by using cathodic arc evaporation technique. This evolution is summarized below.

- A converted layer covering the cathode surface due to phase decomposition forms both for the reactive and nonreactive cases. The arc discharge forms a $TiC_x/TiSi_y/Ti_5Si_3(C)$ multiphase surface.
- The converted layer shows a depth-dependent microstructure in grain size and morphology and also a depth-dependent Si concentration.
- The presence of nitrogen influences the composition of the converted layer by virtue of N uptake into the TiC phase formed by Ti_3SiC_2 decomposition so as to form a cubic TiCN solid solution.
- Variations in arc current values (50–90 A employed here) do not influence the converted layer formation significantly since they all induce local melting of the cathode surface.

ACKNOWLEDGMENTS

The authors acknowledge the financial support from the VINN Excellence Center in Research and Innovation on Functional Nanoscale Materials (FunMat) by the Swedish Governmental Agency for Innovation Systems. The authors also appreciate discussions with Per Eklund and Jun Lu.

[1]S. L. Ma, D. Y. Ma, Y. Guo, B. Xu, G. Z. Wu, K. W. Xu, and P. K. Chu, Acta Mater. **55**, 6350 (2007).
[2]D. V. Shtansky, E. A. Levashov, A. N. Sheveiko, and J. J. Moore, Metall. Mater. Trans. A **30**, 2439 (1999).
[3]R. H. Wei, Surf. Coat. Technol. **203**, 538 (2008).
[4]L. J. S. Johnson, L. Rogström, M. P. Johansson, M. Odén, and L. Hultman, Thin Solid Films **519**, 1397 (2010).
[5]S. Imamura, H. Fukui, A. Shibata, N. Omori, and M. Setoyama, Surf. Coat. Technol. **202**, 820 (2007).
[6]A. Eriksson. J. Q. Zhu, N. Ghafoor, G. Greczynski, J. Jensen, M. P. Johansson, J. Sjölen, M. Odén, L. Hultman and J. Rosén, J. Mater. Res. (2011), DOI: 10.1557/jmr.2011.10.
[7]M. W. Barsoum, Prog. Solid State Chem. **28**, 201 (2000).
[8]P. Eklund, M. Beckers, U. Jansson, H. Hogberg, and L. Hultman, Thin Solid Films **518**, 1851 (2010).
[9]D. Bandyopadhyay, J. Phase Equilib. Diffus. **25**, 415 (2004).
[10]Y. Zhou and W. L. Gu, Z. Metallkd. **95**, 50 (2004).
[11]C. Racault, F. Langlais, and C. Bernard, J. Mater. Sci. **29**, 5023 (1994).
[12]R. Radhakrishnan, J. J. Williams, and M. Akinc, J. Alloys Compd. **285**, 85 (1999).
[13]R. L. Boxman and S. Goldsmith, Surf. Coat. Technol. **33**, 153 (1987).
[14]G. E. Kim, J. L. Meunier, and F. Ajersch, IEEE Trans. Plasma Sci. **23**, 1001 (1995).
[15]B. F. Coll and D. M. Sanders, Surf. Coat. Technol. **81**, 42 (1996).
[16]F. Richter, G. Krannich, M. Kuhn, S. Peter, and C. Spaeth, Mater. Sci. Forum **287–288**, 193 (1998).
[17]J. Rosen, A. Anders, L. Hultman, and J. M. Schneider, J. Appl. Phys. **94**, 1414 (2003).
[18]J. Q. Zhu, A. Eriksson, N. Ghafoor, M. P. Johansson, J. Sjölén, L. Hultman, J. Rosén, and M. Oden, J. Vac. Sci. Technol. A **28**, 347 (2010).
[19]A. Knutsson, M. P. Johansson, P. O. A. Persson, L. Hultman, and M. Odén, Appl. Phys. Lett. **93**, 143110 (2008).
[20]R. M. Langford and A. K. Petford-Long, J. Vac. Sci. Technol. A **19**, 2186 (2001).
[21]W. S. Williams, Prog. Solid State Chem. **6**, 57 (1971).
[22]A. I. Gusev, Russ. Chem. Rev. **65**, 379 (1996).
[23]A. Anders, *Cathodic Arc* (Springer, New York, 2008).
[24]E. D. Wu, E. H. Kisi, S. J. Kennedy, and A. J. Studer, J. Am. Ceram. Soc. **84**, 2281 (2001).
[25]C. S. Park, F. Zheng, S. Salamone, and R. K. Bordia, J. Mater. Sci. **36**, 3313 (2001).
[26]Y. Du and J. C. Schuster, Ber. Bunsenges. Phys. Chem. **102**, 1185 (1998).
[27]N. F. Gao, Y. Miyamoto, and D. Zhang, Mater. Lett. **55**, 61 (2002).
[28]Z. Oo, I. M. Low, and B. H. O'Connor, Physica B **385–386**, 499 (2006).
[29]H. Zhang, Y. Zhou, Y. Bao, and M. Li, J. Am. Ceram. Soc. **91**, 494 (2008).
[30]J. Emmerlich, D. Music, P. Eklund, O. Wilhelmsson, U. Jansson, J. M. Schneider, H. Högberg, and L. Hultman, Acta Mater. **55**, 1479 (2007).